Lab on a Chip

PAPER

View Article Online
View Journal | View Issue

Cite this: *Lab Chip*, 2014, **14**, 3830

A thin-reflector microfluidic resonator for continuous-flow concentration of microorganisms: a new approach to water quality analysis using acoustofluidics†

Dario Carugo,[ab] Tobias Octon,[b] Walid Messaoudi,[b] Adam L. Fisher,[c] Michele Carboni,[c] Nick R. Harris,[d] Martyn Hill[be] and Peter Glynne-Jones*[b]

Received 16th May 2014,
Accepted 5th August 2014

DOI: 10.1039/c4lc00577e

www.rsc.org/loc

An acoustofluidic device has been developed for concentrating vegetative bacteria in a continuous-flow format. We show that it is possible to overcome the disruptive effects of acoustic streaming which typically dominate for small target particles, and demonstrate flow rates compatible with the testing of drinking water. The device consists of a thin-reflector multi-layered resonator, in which bacteria in suspension are levitated towards a glass surface under the action of acoustic radiation forces. In order to achieve robust device performance over long-term operation, functional tests have been carried out to (i) maintain device integrity over time and stabilise its resonance frequency, (ii) optimise the operational acoustic parameters, and (iii) minimise bacterial adhesion on the inner surfaces. Using the developed device, a significant increase in bacterial concentration has been achieved, up to a maximum of ~60-fold. The concentration performance of thin-reflector resonators was found to be superior to comparable half-wave resonators.

1. Introduction

The degradation of water quality can significantly impact on both population health[1,2] and at an industrial level.[3,4] Notably, it has been estimated that poor water hygiene and sanitation cause approximately 3.1% of all deaths and 3.7% of DALYs (Disability Adjusted Life Years) worldwide,[5] with tremendous impact on the cost of healthcare.[6] Microbial contamination in water not only creates domestic and healthcare problems. It can impact on the business performance of industries in diverse fields (*i.e.*, pharmaceutics, chemistry, micro-electronics, food and textile), by severely compromising the quality of finished products.[7] Therefore, accurate and frequent monitoring of microorganisms in water is crucial, and this is also reflected in the progressive tightening of international regulations (*i.e.*, Water Framework Directive).[8]

Currently, the identification and quantification of pathogens in water is mainly performed *via* two-step analysis methods. In these methods a fluid sample is withdrawn from the water supply system (*first step*) and subsequently analysed off-line in a laboratory to identify potential contaminants (*second step*). These methods rely on laborious and time-consuming procedures such as cultural enrichment to increase the number of target microorganisms, or on polymerase chain reaction (PCR) and nucleic acid sequence-based amplification (NASBA) to enrich a single specific DNA or RNA sequence.[9] This poses serious economic and technological limitations to the implementation of routine water analysis procedures in both public and industrial settings,[9] making it difficult to (i) promptly detect the source of microbial contamination, (ii) capture temporal changes in water quality,[10] and (iii) design appropriate and rapid corrective interventions.[11,12] In most cases, the main obstacle in the development of rapid microbial detection methods is represented by the low concentration of microorganisms in water, requiring intermediate off-line laboratory procedures to increase it to a level sufficient for analysis.[13]

Technological advancements are therefore needed to develop on-line water quality analysis systems in which enrichment and detection of microorganisms are carried out within a single technological platform, interfaced with the water supply system. Towards this, microfluidic-based concentrators have been recently developed as an alternative to

[a] *Bioengineering Science Group, Faculty of Engineering and the Environment, University of Southampton, Southampton SO17 1BJ, UK*
[b] *Electro-Mechanical Engineering Group, Faculty of Engineering and the Environment, University of Southampton, Southampton SO17 1BJ, UK. E-mail: P.Glynne-Jones@soton.ac.uk; Tel: +44 (0)2380 595769*
[c] *School of Chemistry, University of Southampton, Southampton SO17 1BJ, UK*
[d] *School of Electronics and Computer Science (ECS), University of Southampton, Southampton SO17 1BJ, UK*
[e] *Institute for Life Sciences (IfLS), University of Southampton, Southampton SO17 1BJ, UK*

† Electronic supplementary information (ESI) available. See DOI: 10.1039/c4lc00577e

classical macro-scale concentration techniques (*i.e.*, centrifugation). The microfluidic environment allows fine manipulation of microorganisms in a continuous-flow format, with unique functional features including optical accessibility, low power consumption, and simplicity of device operation.[14] Furthermore, microfluidic devices offer the possibility of processing biological samples in a closed environment, thus minimising the risk of sample contamination associated with batch handling and centrifugation.[15]

Concentration of bacteria in microfluidic devices has been achieved by different means, including electrical forces,[16–19] hydrodynamic effects,[20] evaporation,[21,22] and ultrasound-enhanced sedimentation.[23] Ultrasound-based external forcing of micro-particles in microfluidics[24] – referred to as acoustofluidics – has recently emerged as a non-invasive way of manipulating cells and particles for a range of applications,[25] such as sample enrichment,[15,26] intra-cellular drug delivery,[27–30] sensing and bio-detection,[31–33] sample filtration,[34–36] cell and particle separation/sorting[37–41] and trapping.[42,43] Continuous-flow concentration of particles in acoustofluidic devices is usually performed *via* generation of an ultrasonic standing wave (USW) within a fluid chamber, causing suspended particles to focus in a confined liquid volume under the action of acoustic radiation forces (ARFs).[44] In order to obtain a significant increase in particle concentration, the fluid flow must be split into the particle-rich and the particle-depleted fractions.[44,45] Based on this functioning principle, concentration of a range of particles including bacterial spores, biological cells and polystyrene spherical microbeads has been demonstrated.[15,38,46–51] Nordin and Laurell have recently demonstrated a very significant increase in concentration of red blood cells and prostate cancer cells (up to a maximum of ~200-fold), using a two-stages half-wavelength resonator.[15]

However, direct manipulation of bodies as small as bacteria by means of ARFs represents a considerable physical challenge.[43] This is mainly due (i) to the fact that the acoustic primary radiation force scales with particle's volume,[45] and (ii) to the increased particle susceptibility with respect to hydrodynamic drag forces resulting from acoustic streaming or thermal convection.[52,53] It has been found that at diameters of around 1 μm there is a transition to drag-dominated behaviour for operating frequencies of ~2 MHz.[52,54] For these reasons, few studies have demonstrated acoustofluidic concentration of flowing particles with diameter <2 μm (ref. 49 and 55) (Table 1). Antfolk *et al.* recently demonstrated focusing of bacteria using a combination of streaming and a two-dimensional resonance; their paper is not included in Table 1, as comparable concentration data was not included; however, impressive performance with polystyrene beads as small as 0.5 μm was shown.[56] Hammarström *et al.* reported on highly efficient static trapping of *E. coli* by half-wave resonance in glass micro-capillaries;[43] they employed 12 μm diameter seed particles to increase the trapping efficiency through the use of secondary, inter-particle ARFs (also known as Bjerknes forces).

In this study we report on the development of an acoustofluidic device for high throughput concentration of microorganisms in a continuous-flow format. The device is based on the thin-reflector arrangement previously described by Glynne-Jones *et al.*,[31] and operates at the first thickness resonance of a composite layered structure. *Escherichia coli K12* and *Staphylococcus epidermidis ATCC 12228* were employed as model microorganisms to assess device performance, and compare it with half-wave resonator design. The significant increase in bacterial concentration achieved with this device, together with the continuous-flow fluid processing, makes it suitable for applications in on-line water quality analysis systems *via* integration with downstream detection units (*i.e.*, optical or bio-chemical). This may open new perspectives in the field of water quality analysis and pathogens detection using acoustofluidics.

2. Theory

2.1 Forces on bacteria in acoustofluidic devices

A spherical particle of static volume V located at a position $\boldsymbol{r}$ within a standing wave field of wavelength λ, will experience a time averaged primary radiation force $F(\boldsymbol{r})$, which is given by:[57]

$$F(\boldsymbol{r}) = V\nabla\left(\frac{3(\rho_p-\rho_m)}{2\rho_p+\rho_m}E_{kin}(\boldsymbol{r}) - \left(1-\frac{\beta_p}{\beta_m}\right)E_{pot}(\boldsymbol{r})\right) \quad (1)$$

Where $E_{kin}(\boldsymbol{r})$ and $E_{pot}(\boldsymbol{r})$ are the time averaged kinetic and potential energy densities, respectively; and ρ and β are the volumetric density and compressibility of the particle (p) or fluid medium (m), respectively.

Of practical interest in acoustic particle manipulation is the so-called acoustic contrast factor (ϕ), which determines the direction and magnitude of the radiation force in a plane standing wave and is given by:

$$\phi = \left(\frac{3(\rho_p-\rho_m)}{\rho_m+2\rho_p} + \frac{\beta_m-\beta_p}{\beta_m}\right) \quad (2)$$

Table 1 Summary of studies reporting on continuous-flow ultrasonic concentration of particles with diameter <2 μm

Author	US field configuration	Flow rate (ml h^{-1})	Particle/cell diameter (μm)	Maximum concentration increase
N. R. Harris *et al.*[49]	Half-wave	6	1 μm (latex bead)	~2.4
R. J. Townsend *et al.*[55]	Quarter-wave	6	1 μm (latex bead)	4.0

For bacteria suspended in a fluid medium ϕ is typically positive,[43] resulting in $F(r)$ being directed towards the pressure nodes of the standing wave (Fig. 1).

In addition to the axial component of the primary acoustic radiation force, a lateral primary acoustic radiation force arises from lateral velocity gradients,[58,59] which translates particles within a plane parallel to the transducer.

From eqn (1) it is evident that the small size of bacteria will result in forces around 1000 times smaller than those experienced by mammalian cells. The difference in volumetric density between bacteria and fluid medium ($\rho_p - \rho_m$, in eqn (2)) is equal to approximately 90 kg m^{-3} for *E. coli*,[60] similar to that found for mammalian cells, such as erythrocytes (~95 kg m^{-3}),[61] lymphocytes (~75 kg m^{-3}),[62] monocytes (~70 kg m^{-3}),[62] or polystyrene beads (~50 kg m^{-3}). Similarly, the differences in compressibility between bacteria, cells and beads will also have an effect but again it will be weaker than that of size.

Generation of an USW in a confined fluidic domain will induce steady fluid motion known as acoustic streaming.[52,63] The outer flow typically takes the form of *Rayleigh streaming*,[63] but we have recently explained other vortex patterns that occur, for example, in the plane of the transducer.[64]

Our strategy for reducing the disruptive effect of streaming in order to concentrate small particles is based on two design features: (a) the Reynolds stresses responsible for the inner streaming patters occur in regions where there are gradients in acoustic energy density.[64] By designing for a uniform field distribution (*e.g.*, by keeping carrier layers thick to prevent flexural modes, and designing for reduced lateral resonances by using sidewalls made from the more acoustically absorbent PDMS rather than Macor), streaming patterns in the transducer's plane are reduced. (b) It may be that the thin reflector design has inherently less *Rayleigh streaming* associated with it, due to the low field gradients found within the fluid layer.[31] Investigation of the streaming patterns in the thin reflector device will be the subject of a subsequent paper.

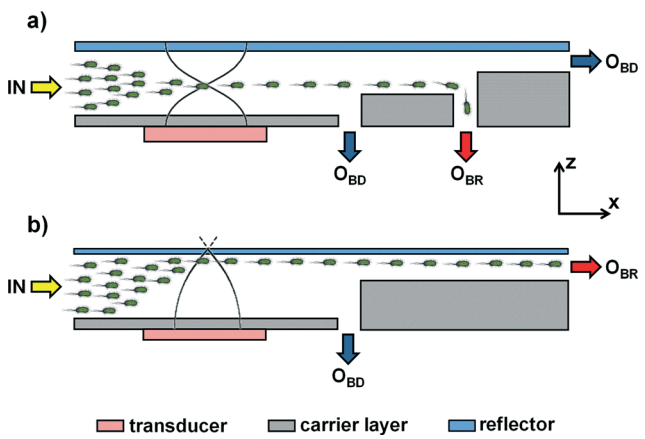

Fig. 1 Functioning principle of half-wave (HW) and thin-reflector (TR) layered resonators. (a) In HW resonators, the fluid layer thickness is ~λ/2 and bacteria are moved by the axial acoustic primary radiation force towards a pressure node located near the mid-plane of the fluid layer (in the *z*-direction). After acoustic focusing is achieved, the fluid flow is split into the bacteria-rich (BR) and the bacteria-depleted (BD) streams. Two interfaces exist between the BR and BD streams. (b) In TR resonators, the fluid layer thickness is $\ll\lambda$ and bacteria are moved by axial acoustic primary radiation force towards a pressure node located at the reflector–air boundary. Only one interface exists between the BR and the BD streams in this case. IN = Inlet; O_{BD} = Bacteria-Depleted Outlet; O_{BR} = Bacteria-Rich Outlet. Layer thicknesses are not to scale.

2.3 Functioning principle of layered acoustic resonators

2.3.1 Half-wave resonator. Planar systems based on the HW resonator were described by Mandralis *et al.* in 1990 and Yasuda *et al.* in 1992 (reviewed in Lenshof *et al.*).[58]

In HW layered resonators the thicknesses of the constitutive layers are typically close to $2n\lambda/4$ (carrier layer), $\lambda/2$ (fluid layer) and $(2n + 1)\lambda/4$ (reflector layer) [n = 0, 1, 2…].[65] This design results in a pressure node located near the mid-plane of the fluid layer, and pressure maxima near the channel walls (Fig. 1a). HW resonators represent the most widely adopted device configuration in continuous-flow acoustofluidics.[36,44,45,58] This acoustic configuration has the advantages of being relatively insensitive to variations in layer thicknesses, and the physical separation achieved between the concentrated sample (*e.g.*, bacteria in suspension) and the inner walls of the fluid chamber is beneficial in sample enrichment applications.

However, since there are particle-depleted layers on both sides of the particle-rich layer, it is difficult to accurately separate the flow into the required partitions. Furthermore, corrugations in the position of the nodal plane[65] mean that a relatively large proportion of particle-depleted fluid must be taken out with the concentrated sample. This is exacerbated by the fact that the particle-rich fluid is at the height of maximum fluid velocity (due to the parabolic flow profile), so by allowing for a small margin of error in the split position a greater volume of particle-depleted fluid is taken than in the thin-reflector case.

2.3.2 Thin-reflector resonator. The TR resonator was described in a study by Glynne-Jones *et al.*[31] It operates at the first thickness resonance of a layered structure, leading to pressure minima located at the solid-air boundaries (Fig. 1b). Compared to the quarter-wavelength resonator, it is more robust to variations in layer thicknesses, and most importantly creates a positive force into the reflector layer at all positions in the channel.[66] The terms 'reflector' and 'carrier' are less accurate as descriptions of layer functions in this case,[31] however these terms will be retained to aid clarity. The reflector and fluid layers thicknesses are much less than the acoustic wavelength, causing particles in the fluid medium to be attracted in the direction of the reflector–air interface.[65] However, physical contact between the processed biological sample and the reflector surface (typically glass) may result in the occurrence of sample adhesion to the surface, and potentially bio-fouling after long-term operation. Ultrasound-induced deposition of cells has application in

immunologically based detection;[33] its occurrence is generally undesired in continuous-flow concentrators.

3. Materials and methods

3.1 Devices design and fabrication

A 1-D transfer impedance model implemented in MATLAB® (The MathWorks Inc., USA) was employed to predict the approximate position of the pressure nodes and define the thickness of each layer.[67,68]

A similar design and fabrication strategy was adopted for both HW and TR resonators (Fig. 2), which mainly differed in the thickness of the constitutive layers (see Table 2 for layers thickness values). A 17.0 mm × 35.5 mm × 1.0 mm PZT transducer (PZ26, Ferroperm Piezoceramics, Denmark) was coupled to the carrier layer by using epoxy (Epotek 301, Epoxy Technology, Inc., USA) cured at 80 °C for 2 h. The carrier layer was milled from Macor (Ceramic Substrates & Components Ltd, UK), a machinable ceramic material. The walls of the fluidic chamber were formed by a custom moulded polydimethylsiloxane (PDMS) gasket (Sylgard® 184, Dow Corning Corporation, USA) (Fig. 2a). This was obtained by mixing PDMS precursor and curing agent (10 : 1 w/w), followed by degassing, and curing at 70 °C for 1 h.

The thickness of the fluid chamber in the active region (*i.e.*, above the transducer) was equal to 0.10 mm (TR) and 0.38 mm (HW), whilst channel width was identical in both devices and equal to 12.00 mm. The reflector layer was formed by a 75 mm × 25 mm × 1 mm glass slide (Fisher Scientific Ltd., USA) in the HW device, and a 75 mm × 25 mm × 0.17 mm glass coverslip (Logitech Ltd., Scotland) in the TR device. Notably, the thickness of the reflector layer in TR device was equal to 0.024λ.

A milled poly(methyl methacrylate) (PMMA) manifold permitted fluidic connectors to deliver the fluid sample into the chamber and to withdraw the bacteria-rich and bacteria-depleted samples (Fig. 2a and b). For this purpose, connection ports with 1/4-28 flat-bottom thread were created through the PMMA layer to join the end of each channel with 1/16" outer diameter tubing (Fig. 2b). Ports were sealed using custom moulded PDMS gaskets. A steel clamp held the glass to the other layers, with a window for optical accessibility (Fig. 2a).

Photographs of the HW and TR devices and the individual components are shown in Fig. 2. The HW device had three outlet ports, one for the collection of the bacteria-rich fluid and two for the discharge of the bacteria-depleted fluid, while in the TR device only one outlet port was required for discharging the bacteria-depleted fluid.

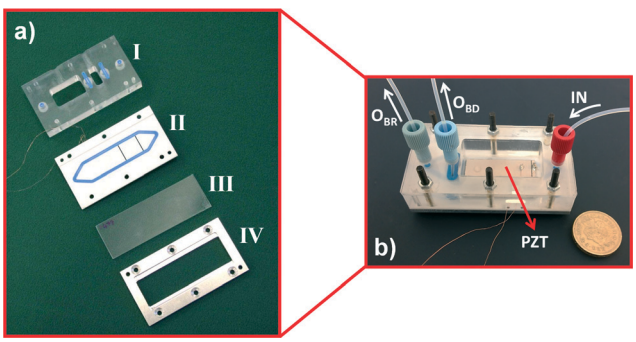

Fig. 2 (a) Exploded view of an acoustic resonator. This comprises of (I) a PMMA manifold for connection of inlet/outlet tubing, (II) a milled Macor HW carrier layer (white) which has a recess to define the fluid channel, and a groove for the PDMS gasket (blue) which defines the extent of the fluid channel, (III) a glass reflector, and (IV) a metal frame with a window for optical accessibility. (b) Assembled TR device, with inlet/outlet tubing and a PZT element (red arrow) coupled to the carrier layer. The white arrows indicate the flow direction at the inlet and outlets of the device. IN = Inlet; O_{BD} = Bacteria-Depleted Outlet; O_{BR} = Bacteria-Rich Outlet.

3.2 Instrumental setup

The ultrasonic transducer was actuated by an in-house constructed power amplifier driven by a sine-wave from a programmable signal generator (TG1304, Thurlby Thandar Instruments, UK). A digital storage oscilloscope (DSO1152B, Agilent Technologies, USA) was used to monitor the applied voltage and the operating frequency. The latter was determined from electrical impedance measurements (impedance analyser: C-60, Cypher Instruments Ltd., UK, measurements at 2 V_{pp}).

Microscopy image sequences were acquired using an epi-fluorescence microscope (BXFM, Olympus Corporation, Japan) and CCD camera (Pixelfly, PCO AG, Germany). The microscope was also equipped with:

– controller of objective *z*-position (ES10ZE, Prior Scientific Instruments Ltd., UK);

– controller of stage *x*–*y* position (MLS203-1, Thorlabs, USA).

Image acquisition and position control were carried out *via* Micro-Manager open-source microscopy software.[69]

3.3 Experimental setup

A schematic of the experimental setup for the functioning of HW and TR resonators is reported in Fig. 3a and b, respectively.

PTFE tubing, inner diameter 500 μm (1/16" OD, Upchurch Scientific, USA), was employed to connect the device inlet and outlets. Gas tight glass syringes (Hamilton Bonaduz AG, Switzerland) were mounted on syringe pumps (*inlet*: KD100, KD Scientific Inc., USA; *outlets*: Pump 11 Elite, Harvard Apparatus, USA). For the results presented here, fine control over the volumetric flow rates was achieved by using syringe pumps on all inlet and outlet lines, except for those cases when $O_{BR}/O_{IN} > 0.03$ when sufficient control could be achieved by leaving O_{BR} open ended which made sample collection easier. Using less than two pumps and controlling the flow ratios by passive means such as controlling flow resistance in the outlet lines was not explored in this work; we envisage this might be problematic as any fouling of the lines could disrupt the intended flow ratios. A small air plug was

Table 2 Dimensional and physical properties of HW and TR resonators. Thickness values refer to those in the active region of the device. The thickness normalised to the US wavelength (λ) was calculated considering a resonant frequency (f_R) of 1.46 MHz and 826 kHz for HW and TR, respectively. The velocity of sound was set to 4529.8 m s^{-1} (transducer), 5510 m s^{-1} (carrier), 1480 m s^{-1} (fluid) and 5872 m s^{-1} (reflector). The width of the fluid layer = 12 mm

	Layer	Thickness (μm)	Thickness/λ	Material	Density (kg m^{-3})
HW resonator	Transducer	1000	0.322	PZ26 (Ferroperm)	7700
	Carrier	200	0.053	Macor	2540
	Fluid	380	0.375	PBS	~1000
	Reflector	1000	0.249	Glass	2500
TR resonator	Transducer	1000	0.182	PZ26 (Ferroperm)	7700
	Carrier	980	0.147	Macor	2540
	Fluid	100	0.055 ($\ll\lambda$)	PBS	~1000
	Reflector	170	0.024 ($\ll\lambda$)	Glass	2500

left within the syringes, which acted as a damper of the pressure wave generated by the stepper motor of the pump. Steady and predictable fluid flow within the device is preferred to achieve the desired performance, although devices are predicted to operate effectively within a certain degree of flow pulsatility.[49] An additional fluidic line was connected *via* a 3-way valve (Upchurch Scientific, USA) to the inlet line for de-bubbling the chamber by flushing with 100% carbon dioxide (CO_2) as described below. Shut-off valves (Upchurch Scientific, USA) were installed on each outlet line in order to selectively control liquid/gas distribution within the device.

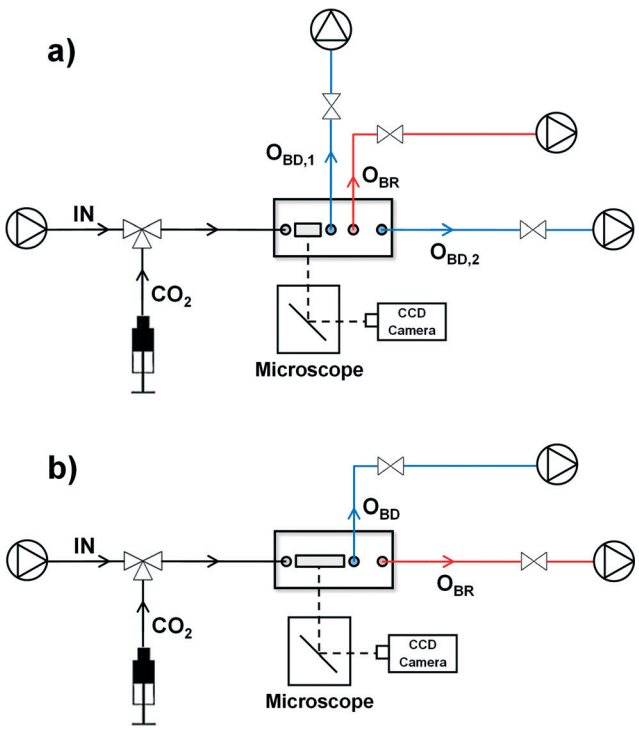

Fig. 3 Experimental setup for (a) HW and (b) TR devices. Fluid injection and withdrawal was achieved by means of syringe pumps. Carbon dioxide (CO_2) was manually injected during the procedure of bubbles removal from the fluid layer of the device. Devices were placed on a microscope stage for optical assessment of bacteria levitation. A CCD camera was coupled with the microscope for image acquisition. IN = Inlet; O_{BD} = Bacteria-Depleted Outlet; O_{BR} = Bacteria-Rich Outlet.

3.4 Experimental protocols

3.4.1 Model microorganisms. Device performance was assessed using *Escherichia coli* (*E. coli*) *K12* (Bio-Rad Laboratories, Inc., USA) and *Staphylococcus epidermidis* (*S. epidermidis*) *ATCC 12228* as model microorganisms. Bacteria were fluorescently stained with a bacterial viability kit (LIVE/DEAD® *Bac*Light™, Invitrogen Corporation, USA) in order to visualise them under the microscope. Protocols for bacteria culturing and staining are reported in ESI† S1. Fluorescent microscope images of bacteria were acquired and transferred to ImageJ open-source software[70] for bacterial counting using the built-in *Analyze Particles* function.

3.4.2 Devices operation protocols. Air bubbles trapped within the device can significantly compromise its acoustic and hydrodynamic performance. See ESI† S2 for details of how CO_2 was used to remove bubbles.

After complete bubble removal was achieved, the device was primed with PBS. The stained bacterial suspension (10 ml) was delivered *via* the syringe pump. As the pump was started, the ultrasonic signal was applied.

3.4.3 Optimisation of the ultrasonic operating conditions. Selection of the devices' ultrasonic operating conditions (*i.e.*, US frequency and amplitude) was carried out through experimental optimisation of the acoustic levitation performance (Fig. 4), as follows:

(i) the device was placed on the microscope stage and the field of view positioned just after the active region (~1 mm from the transducer edge, in the *x*-direction), and centrally with respect to the fluidic chamber (*i.e.*, in the *y*-direction);

(ii) bacteria were injected into the device and US was activated;

(iii) both inlet/outlet flow rates and US were deactivated, and the region of interest was scanned in the *z*-direction (*i.e.*, perpendicular to the main flow direction) by acquiring equally-spaced microscope images of bacteria at a pre-set spatial resolution (Δz);

(iv) the number of bacteria in each image frame was counted (see above) and the % number of bacteria plotted as

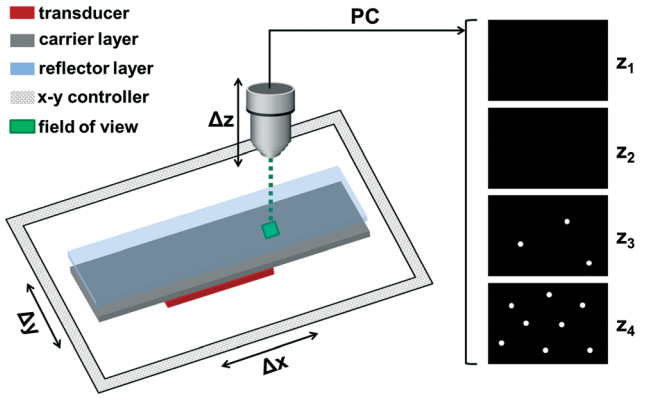

Fig. 4 Experimental optimisation of the ultrasonic operating parameters. "z-Scan": a controller of objective z-position was employed to acquire microscope images of bacteria across the fluid layer thickness (*i.e.*, from the carrier layer, at $z = z_1$, to the reflector layer, at $z = z_4$), at a given spatial resolution (Δz). Image processing quantified the % number of bacteria *vs.* z-position, and assessed the acoustic levitation performance. An x–y stage position controller was employed to accurately move the microscope stage (and thus the microscope field of view) and assess the acoustic performance along the full width of the fluid layer. This was particularly useful to assess the levitation performance near the edges of the fluid chamber.

a function of the z-position, in order to assess the distribution of bacteria through the height of the device.

3.4.4 Stabilisation of the reflector layer in TR device. In TR device, the reflector layer was found to be susceptible to bending due to hydraulic pressure (and potentially acoustic radiation forces). This bending becomes worse if the device is a single unit of a more complex system, in which multiple fluidic connections are required between each individual unit thus increasing the overall hydraulic resistance. The bending causes unwanted shifts of the resonant frequency (and occasionally reflector rupture if micro-cracks are already present in the glass layer). Initially, both complications were observed; in our final design the glass was supported by three equally-spaced transversal bars (~1.5 mm wide) in the window of the metal clamp. The inter-spacing between bars was equal to approximately 17.0 mm, and they crossed the optical window for the entire width of the fluid chamber (see ESI† S2).

In order to assess the robustness of this design, electrical impedance measurements were taken while the inlet fluid flow rate (Q_{IN}) in the chamber was increased from 0 to 40 ml h^{-1}, and maintained for a maximum of 1 h at each flow rate. The resonant frequency was found to be stable over this range of flow rates.

3.4.5 Minimisation of bacteria attachment on the reflector surface in TR device. In TR device bacteria were forced towards the reflector–liquid interface. When making contact, bacteria can reversibly or irreversibly adhere to the hydrophilic surface of the glass;[71] this compromises device performance. The mechanisms governing bacteria interaction with treated and untreated glass surfaces are multifarious, and have been the subject of investigation for many researchers in the fields of bio-fouling and development of antimicrobial substrates.[72–74] In TR devices bacteria attachment depends on many factors including the interplay between a range of physico-chemical properties, such as surface chemistry and roughness, and also the strength of the acoustic force directing them towards the surface. Although an investigation of these mechanisms is currently underway in our laboratories, in the present study we explored the use of a range of surface treatments to minimise bacterial attachment on the glass reflector of TR device (data to be published at a later date). These included hydrophobic coatings and polymer brushes. Among the different surface treatments investigated, coating with hydrophobic silane was found to be effective in minimising bacterial adhesion. The coating was performed as follows: the glass slide was cleaned with isopropyl alcohol (Sigma Aldrich Corporation, USA), rinsed with deionised water (Millipore Corporation, USA) and dried in an oven at 60 °C for 1 h. The slide was then immersed in a solution of trichloro(1*H*,1*H*,2*H*,2*H*-perfluorooctyl)silane (5% v/v in anhydrous *N*,*N*-dimethylformamide) to initiate a condensation reaction between the silane and the hydroxyl groups on the glass surface. Subsequently, the glass surface was washed several times with ethanol, deionised water, and dried with compressed air.

3.4.6 Performance assessment of TR device. The devices' ability to increase bacterial concentration was assessed by optical bacterial counting. In this set of experiments, the initial concentration of bacteria was set to 10^4 CFU ml^{-1} and quantified *off-chip* prior to each test run. The final concentration of bacteria was quantified by two means: (i) at flow rate ratios $Q_{BR}/Q_{IN} > 0.02$, the concentrated bacterial suspension was collected and bacteria counted *off-chip*; and (ii) at $Q_{BR}/Q_{IN} \leq 0.02$, bacteria were counted *on-chip* by acquiring microscope images in correspondence to the device outlet port (O_{BR}). No significant bacterial loss due to attachment/sedimentation in the outlet tubing occurred at the higher Q_{BR}/Q_{IN}; thus the two methods can be considered nearly equivalent.

Bacteria were counted from the acquired microscope images. The increase of bacteria concentration (IC) was calculated as an indication of device performance:

$$\mathrm{IC} = \frac{C_{BR}}{C_{IN}} \quad (3)$$

Where C_{BR} and C_{IN} are the concentration of bacteria at the bacteria-rich outlet and at device inlet, respectively.

3.4.7 Effect of initial bacterial concentration on TR performance. Given the large variability of bacterial concentration in water supply systems, it is particularly important to evaluate the performance of TR device under variable concentrations of bacteria in the processed water sample. For this purpose, *E. coli* were suspended in PBS at different concentrations (C_{IN} = 10, 10^2, 10^3 and 10^4 CFU ml^{-1}) and device performance (*i.e.* increase in the bacterial

concentration, IC) under these operational conditions was assessed. For these specific experiments, the inlet flow rate (Q_{IN}) was set to 20 ml h^{-1} and Q_{BR}/Q_{IN} was set to 0.05. Given the difficulty associated with *off-chip* counting of bacteria at the lower bacterial concentrations (particularly at $C_{IN} < 10^3$ CFU ml^{-1}), bacteria were individually tracked under the microscope and the percentage number of bacteria flowing above the bacteria-depleted outlet was quantified to assess device performance. Measurements were taken at two different *y*-positions, one located approximately at the centre of the fluid chamber and the other located in close proximity to the side wall. Device performance in the central region (IC_{CENT}) and in the lateral region (IC_{LAT}) of the fluid chamber was determined. The overall device performance (IC) was estimated from the weighted average of IC_{CENT} and IC_{LAT}, as follows:

$$IC = \left(\frac{1}{3}\cdot IC_{LAT}\right) + \left(\frac{2}{3}\cdot IC_{CENT}\right) \quad (4)$$

Where the parameters of the weighted average have been derived from measurements across the device width (described below, see Fig. 9b), which show that TR device performance is lower near the side walls of the fluid chamber and reaches a plateau at a distance of ~2 mm from the channel side wall. This phenomenon – referred to as an 'edge effect' – thus affects approximately 1/3 of the fluid chamber total width.

3.4.8 Assessment of the spatial uniformity of the ultrasonic field. The capability of achieving spatially even acoustic levitation of bacteria in the fluid layer across the width of the device was assessed, with the aim of identifying potential sources of performance degradation and design corrective strategies for a second generation of bacterial concentrators. A *z*-scan analysis (see steps i–iv in section 3.4.3) was performed at a range of positions across the full width of the fluid chamber (*i.e.* taking consecutive images over a range of *z*-positions using the focus drive on the microscope, then repeating this over a range of positions across the device), at a fixed *x*-position and with varying the *y*-position by means of an *x*–*y* stage controller (Δy = 400 μm). Fluid flow rate and US were re-activated in between individual *z*-scans, so as to ensure that each acquisition was performed under identical conditions.

Both HW and TR devices were investigated with this method.

4. Results and discussion

4.1 Verification and stabilisation of the resonance frequency

In order to experimentally determine the operating frequency of the developed resonators, electrical impedance measurements were performed using an impedance analyser. Series resonances were found at 1.46 MHz and 826 kHz for the HW and TR device, respectively.

The effectiveness of the bars introduced to prevent bending of the reflector layer described above was investigated. For this purpose, electrical impedance was measured at varying fluid flow rates in the range 0–40 ml h^{-1}. Fig. 5c shows impedance plots at Q_{IN} = 0 ml h^{-1}, 40 ml h^{-1} (maintained for 1 h) and 0 ml h^{-1} (end-point). Results show that the impedance minimum slightly shifted to a lower frequency when the flow rate was increased from 0 ml h^{-1} (~831 kHz) to 40 ml h^{-1} (~822 kHz), likely due to a dilation of the fluid layer caused by the increased hydraulic pressure. However, when the flow rate was stopped (0 ml h^{-1}, end-point), the position of the impedance minimum retained its shifted value, signifying that the device was stabilised in its final configuration. Fig. 5d shows the % deviation of the frequency at minimum impendence, measured at Q_{IN} = 10, 20, 30 and 40 ml h^{-1}. This was calculated with respect to the average value; thus positive/negative values correspond to an increase/reduction of the frequency with respect to the average value. Results show that the frequency of minimum impedance was substantially independent from the flow rate applied (*i.e.*, maximum 0.089% variation), further corroborating the effectiveness of the stabiliser bars in the metal frame to prevent deformation of the thin glass reflector layer during long-term operation.

Physical stabilisation was not required in HW devices, in which the thickness of the reflector layer was ~6 times greater than in TR devices.

4.2 Optimisation of TR device acoustic operating parameters

In order to achieve robust device functioning and minimise the risk of device going out-of-resonance over extended operating periods, frequency sweeping was applied. This approach brings with it a range of benefits such as reduced temperature dependence, less need for controlling the driving frequency and uniformity of the force field within the acoustic chamber.[75]

The selection of the optimal frequency range was assessed by performing a *z*-scan analysis (as described above, Δz = 5 μm), at fixed frequencies in the range 816–836 kHz, with a frequency resolution of 1 kHz. The inlet flow rate (Q_{IN}) was set to 20 ml h^{-1} and the peak-to-peak voltage (V_{pp}) to 20 V. *E. coli* was employed for this characterisation, and was injected into the device at a concentration of ~10^4 CFU ml^{-1}. At each individual frequency, the % number of bacteria located within a fluid layer 10 μm from the reflector surface was quantified (Fig. 6a). Fig. 6b shows that for frequencies in the range 823–828 kHz this value was >90%, whilst it slightly reduced at frequencies <823 kHz (*i.e.* down to 85.8 ± 0.7%, at f = 816 kHz) and decreased more significantly at frequencies >828 kHz (*i.e.* down to 76.2 ± 0.6%, at f = 836 kHz). The frequency range 823–828 kHz was thus selected as the optimal range for sweeping, and a sweep period of 50 ms was applied.

Optimisation of the operating voltage was carried out by performing *z*-scan analysis at peak-to-peak voltages in the

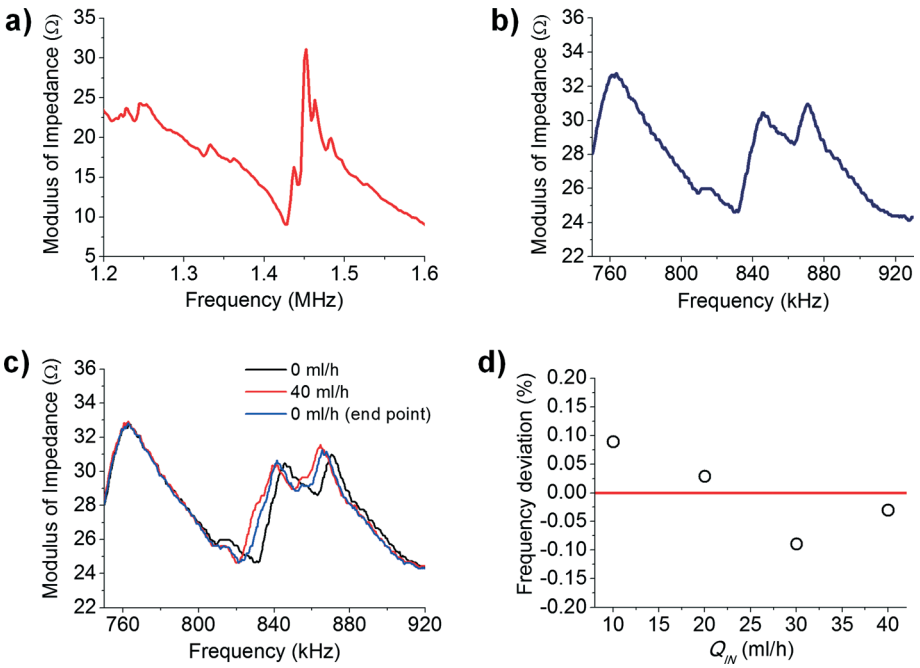

Fig. 5 Verification and stabilisation of the resonance frequency. (a–b) Electrical input impedance for fluid-filled HW (a) and TR (b) resonator, determined experimentally under static fluidic condition. Impedance minima were at f_R = 1.43 MHz (HW) and f_R = 831 kHz (TR). (c) Electrical input impedance for TR resonator, at Q_{IN} = 0 ml h^{-1}, 40 ml h^{-1} and 0 ml h^{-1} (end-point). (d) % Deviation of the frequency at minimum impedance, calculated with respect to the average frequency (red line), at Q_{IN} = 10, 20, 30 and 40 ml h^{-1}. Positive/negative values correspond to an increase/reduction of the frequency at minimum impedance with respect to the average value.

range 0–28 V_{pp} (at Q_{IN} = 20 ml h^{-1}). A frequency sweep was applied, in the optimised range 823–828 kHz (sweep period: 50 ms). Fig. 6c shows that the effectiveness of ultrasonic bacteria levitation increased with increasing the applied voltage, due to the corresponding higher acoustic radiation forces exerted on bacteria, with maximal levitation effectiveness achieved at 22 V_{pp}. At $V_{pp} > 24$ device performance significantly reduced. An optimal operating voltage of 22 V_{pp} was thus selected from these investigations. The source of performance degradation at the higher voltages has not been fully identified yet, and could be potentially attributed to (i) increased acoustic streaming velocities, (ii) subtle temperature changes causing a deviation of the resonance frequency, or (iii) increased lateral radiation forces causing augmented local bacterial concentration (*i.e.*, inter-bacterial competition to occupy a narrow region of the acoustic field). In the ideal case, both streaming velocity and acoustic radiation force would scale with the square of the acoustic pressure amplitude. This would lead to higher throughputs being achievable by increasing the supply voltage. However other factors might interfere with this such as heating and hydrodynamic effects. We did not test this hypothesis in our experiments as 20 ml h^{-1} was sufficient for our intended application. Investigating the streaming patterns directly has proved difficult since auto-fluorescence of the Macor device walls creates a background against which it's hard to see submicron tracer particles. The motion of larger tracer particles is dominated by acoustic radiation forces rather than streaming drag forces.

The HW was found to be more sensitive to variations in the driving frequency, compared to the TR resonator. A similar optimisation of the operating acoustic parameters was performed for HW devices (data not shown). An optimal frequency sweep range of 1.4585–1.4615 MHz (sweep period = 50 ms) and peak-to-peak voltage of 2.8 V were identified. Notably, 1-D transfer impedance modelling predicts a similar acoustic pressure gradient across the fluid layer of TR and HW devices under the optimised experimental conditions.

4.3 Concentration performance of TR resonator

Fig. 7a shows the increase in bacterial concentration (IC) achieved with TR device, at Q_{BR}/Q_{IN} ranging from 0.0025 to 0.2, and Q_{IN} = 20 ml h^{-1}. The acoustic operational parameters were set to the optimised values. *E. coli* was used as a model microorganism for these experiments, at C_{IN} ~ 10^4 CFU ml^{-1}.

Experimental values are compared with the theoretical values, calculated assuming that all bacteria are directed into O_{BR} as a result of ideal acoustic manipulation. The percentage difference between experimental and theoretical values is reported in Fig. 7b, as a function of Q_{BR}/Q_{IN}.

Results show that the TR device is capable of achieving significant increase in bacterial concentration, which ranges from 3.8 ± 0.5 (at Q_{BR}/Q_{IN} = 0.2) up to a maximum of 60.0 ± 7.4 (at Q_{BR}/Q_{IN} = 0.005) (Fig. 7a). To the best of our knowledge, this is the highest increase in bacterial concentration reported to date using a continuous-flow acoustofluidic device. However, at $Q_{BR}/Q_{IN} < 0.005$, TR performance was

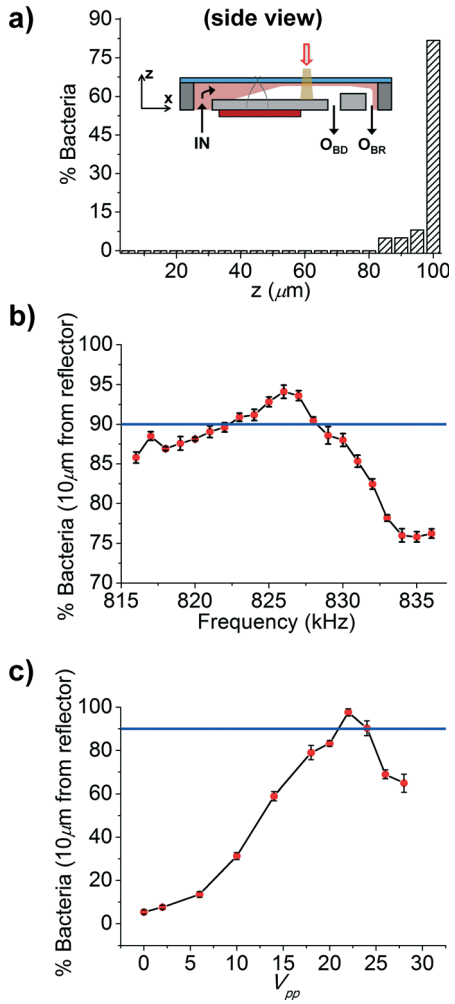

Fig. 6 Identification of TR device acoustic operating parameters. (a) Representative result of a *z*-scan analysis in TR resonator. The % number of bacteria (*E. coli*) is determined at different *z*-positions, ranging from z = 0 μm (carrier layer) to z = 100 μm (reflector layer), with a spatial resolution (Δz) of 5 μm. The field of view of the microscope is located centrally with respect to the fluid chamber (in the *y*-position), and ~1 mm downstream of the PZT element. The majority of bacteria are located at the reflector surface (~81%), and the % of bacteria located within 10 μm of the reflector surface is >90%. Q_{IN} = 20 ml h^{-1}. (b) % Bacteria located in a fluid layer 10 μm from the reflector surface, as determined from *z*-scan analysis, at varying operating frequencies in the range 816–836 kHz. Q_{IN} = 20 ml h^{-1}, 20 V_{pp}. n = 3. (c) % Bacteria located in a fluid layer 10 μm from the reflector surface, as determined from *z*-scan analysis, at varying peak-to-peak voltages in the range 0–28 V_{pp}. f = 823–828 kHz (sweep period = 50 ms), Q_{IN} = 20 ml h^{-1}. n = 3. The red line in (b) and (c) corresponds to 90% bacteria located in a fluid layer 10 μm from the reflector surface.

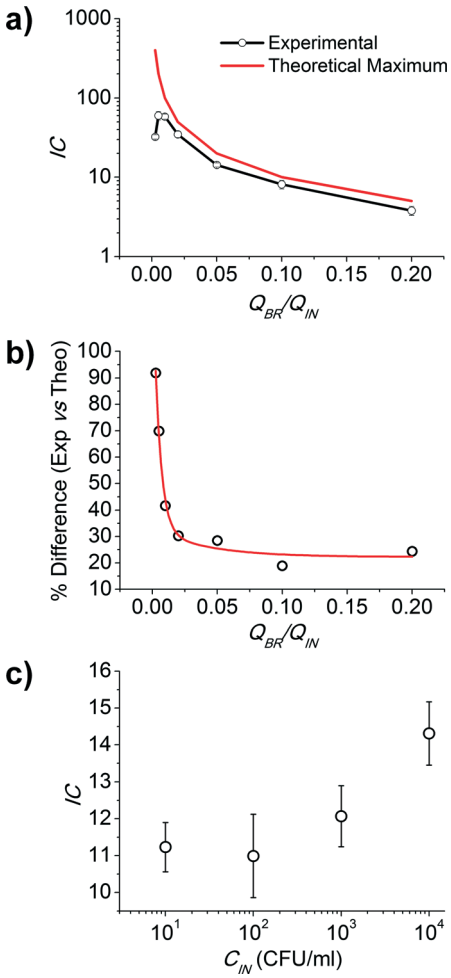

Fig. 7 Concentration performance of TR resonators. (a) Bacteria concentration increase (IC) achieved with TR device (Q_{IN} = 20 ml h^{-1}) at varying Q_{BR}/Q_{IN}. Experimental values (n = 3) are compared with theoretical values. C_{IN} = 10^4 CFU ml^{-1}. *Y*-axis is in log scale. (b) % Difference between experimental and theoretical IC values, at varying Q_{BR}/Q_{IN}. This was calculated as % difference = $[(|IC_{Exp} - IC_{Theo}|)/IC_{Theo}] \times 100$. The red line corresponds to exponential interpolation of the data points. (c) Bacteria concentration increase (IC) achieved with TR device (n = 2), at different initial concentrations of *E. coli* in the inlet suspension (C_{IN}). Q_{IN} = 20 ml h^{-1}; Q_{BR}/Q_{IN} = 0.05. *X*-axis is in log scale.

observed to abruptly decrease (Fig. 7a and b) likely due to a significant number of bacteria escaping the bacteria-rich layer, caused by insufficient radiation force to constrain the bacteria in a fluid layer as thick as the characteristic bacterial size. Furthermore, by comparing experimental with theoretical values (Fig. 7a and b), it appears evident that there is still a large margin for performance improvement. Notably, whilst the device was observed to perform effectively in the central region of the fluidic chamber, a loss of performance was observed in close proximity to the channel side walls. Other sources of performance degradation may include bacteria sedimentation in the syringe or attachment on the tubing inner surfaces, particularly in the long-term and at the lower Q_{BR}/Q_{IN}.

Table 3 reports the concentration increase (IC) achieved with using TR and HW resonators at Q_{IN} = 20 ml h^{-1} and Q_{BR}/Q_{IN} = 0.2, 0.1 and 0.05. Results show that at the higher Q_{BR}/Q_{IN}, the two resonators performed similarly (percentage difference in concentration increase: 24.3%). However, with reducing Q_{BR}/Q_{IN}, the TR configuration displayed a significantly higher IC compared to the HW configuration. The concentration factor for the HW device reached a maximum of

Table 3 Concentration increase (IC) achieved with HW and TR devices, at Q_{IN} = 20 ml h^{-1}, Q_{BR}/Q_{IN} = 0.05–0.2, and C_{IN} = 10^4 CFU ml^{-1} (n = 3). Bacterial recovery rates (%) for TR device are reported (n = 3)

Q_{BR}/Q_{IN}	IC half-wave	IC thin-reflector	Recovery rates thin-reflector (%)
0.2	3.0 ± 0.5	3.8 ± 0.5	75.6 ± 9.8
0.1	3.4 ± 0.2	8.1 ± 1.0	81.1 ± 10.2
0.05	3.0 ± 0.4	14.3 ± 0.9	71.6 ± 4.3

3.4 at Q_{BR}/Q_{IN} = 0.1 and reduced to 3.0 at Q_{BR}/Q_{IN} = 0.05; likely due to an increased number of bacteria escaping the top and bottom outlets of the device. Bacterial recovery rates for TR device, at practical $Q_{BR}/Q_{IN} \geq 0.05$, were greater than 70%. Results show that the TR device is capable of achieving significantly higher concentration increase (maximum of ~1 order of magnitude) compared with traditional HW configurations. The latter performed similarly to previously reported half-wave or quarter-wave devices.[49,55]

Among the potential factors causing reduced performance of layered HW resonators compared to TR resonators are: (i) geometrical distortions of the nodal plane causing bacteria to reach the flow split at different z-positions,[48] (ii) presence of two interfaces between the bacteria-rich and the bacteria-depleted streams, and (iii) strong lateral variations of the acoustic intensity.[31] Results confirm the potential of TR resonators to be employed as concentrators of micro-particles and microorganisms, as an alternative to traditional HW layered resonators.

4.4 Effect of initial bacterial concentration on TR device performance

Fig. 7c shows the increase in bacterial concentration (IC) achieved using the TR device (at a fixed Q_{BR}/Q_{IN} = 0.05), at varying initial concentrations of bacteria in the inlet suspension (C_{IN}), corresponding to 10, 10^2, 10^3 and 10^4 CFU ml^{-1}. eqn (4) was used to calculate IC at the lower bacterial concentrations.

Results show that measured device performance slightly decreased with reducing the initial bacterial concentration from 10^4 CFU ml^{-1} (IC = 14.3) down to 10^3 CFU ml^{-1} (IC = 12.1). Notably, TR performance remained substantially invariant with further decreasing bacterial concentration (*i.e.*, IC = 11.2, at C_{IN} = 10 CFU ml^{-1}), and likely no statistical difference in performance subsists at these lower initial concentrations ($C_{IN} < 10^4$). Increased performance at the higher C_{IN} may be attributed to the effect of acoustic secondary radiation forces, which can cause clumping of bacteria at higher concentrations making them easier to manipulate. However, it should be noted that approximations in the determination of IC at the lower C_{IN}, may have caused inaccuracies in the calculation of TR performance.

Despite approximations in the measurements, results demonstrated that TR device is capable of achieving significantly high concentration increase under a wide range of bacterial concentrations in the inlet suspension, making it suitable for applications where a variable microbial load in water is present.

4.5 Comparison between *E. coli* and *S. epidermidis*

In order to assess the capability of TR resonator to acoustically levitate and concentrate different bacterial species, comparative tests were performed using both *E. coli* and *S. epidermidis*. z-Scan analyses were carried out for this purpose, at Q_{IN} = 10 and 20 ml h^{-1}. Fig. 8 shows the % number of bacteria located within a fluid layer 10 μm from the reflector surface, for both *E. coli* and *S. epidermidis*. Results show that TR resonator was capable of effectively levitating both bacterial species towards the reflector surface, with no significant difference between the two species. Notably, the two bacterial species have comparable average cell volume, in the range 0.5–0.7 μm^3. A marginal decrease in performance was observed with increasing the inlet flow rate from 10 ml h^{-1} to 20 ml h^{-1}, likely due to the reduced exposure of bacteria to the acoustic field at the higher flow rate.

4.6 Assessing the spatial uniformity of the acoustic levitation performance

A potential source of performance degradation has been identified in the reduced strength of the ultrasonic field in regions of the fluid layer located in close proximity to the side walls of the device. Despite weakening of the acoustic field near the edges of acoustic resonators has been previously reported,[76] the underlying physical mechanisms have not been clearly identified yet. Furthermore, a quantification of this effect (referred to as 'edge effect') has not been previously reported. This is a necessary prerequisite for

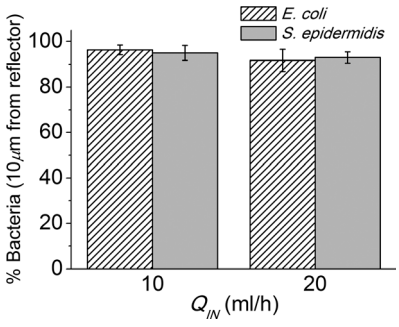

Fig. 8 Ultrasonic levitation of *E. coli* and *S. epidermidis* in TR resonator. Average % number of bacteria located within 10 μm of the reflector at Q_{IN} = 10 and 20 ml h^{-1} (n = 3). C_{IN} = ~10^4 CFU ml^{-1}. f = 823–828 kHz (sweep period = 50 ms), 22 V_{pp}.

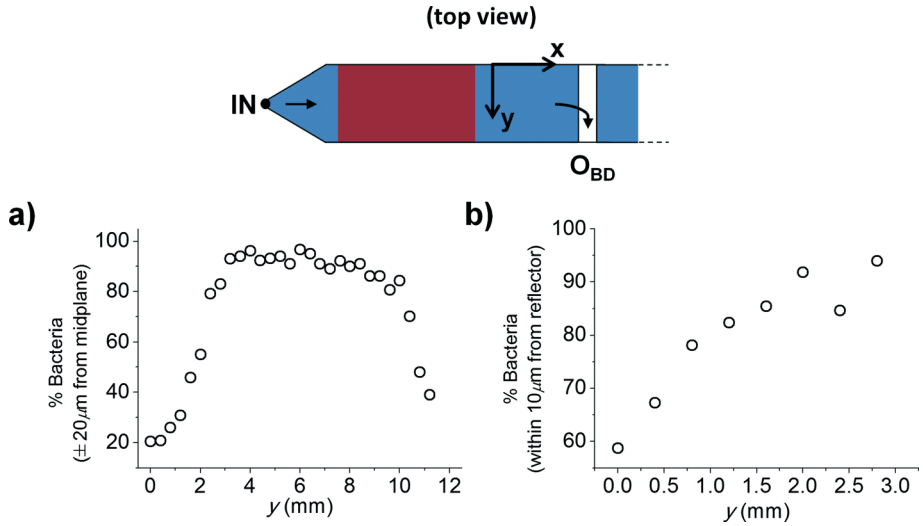

Fig. 9 Assessing the spatial uniformity of the acoustic levitation performance. (a) % Bacteria located less than 20 μm from chamber mid-plane at different *y*-positions across the width of the fluid layer of a HW device. (b) % Bacteria located within 10 μm from the reflector at different *y*-positions across the width of the fluid layer of a TR device. The acoustic parameters correspond to the optimised frequency sweep range and peak-to-peak voltage.

implementing corrective strategies and improving the performance of acoustic concentrators. For this purpose, *z*-scan analyses have been performed across the full width of the fluid layer, using *x*–*y* stage controller which allowed to precisely changing the position of the microscope field of view.

Fig. 9a shows the % number of bacteria (*E. coli*) located in a 40 μm thick fluid layer (centred on the chamber mid-plane) at different *y*-positions (Δy = 400 μm), in the HW resonator. Objective *x*-position was fixed and set to 0.6 mm from the transducer edge. It can be observed that device performance was significantly reduced in proximity to the side walls of the chamber (down to a minimum of ~20%), with highly asymmetric characteristics. Conversely, in the central region of the device bacteria were effectively constrained to a relatively narrow fluid layer under the action of radiation forces. Notably, the 'edge effect' was observed to occupy a larger portion of the fluid layer width than for the TR device, which may have limited the maximum concentration increase achievable with HW layered resonators.

Fig. 9b shows the % number of bacteria (*E. coli*) located in a 10 μm thick fluid layer (from the reflector surface) at different *y*-positions (Δy = 400 μm), in the TR resonator. Objective *x*-position was fixed and set to 0.6 mm from the transducer edge. Results are reported up to 2.6 mm from the chamber side wall, after which the performance was substantially invariant. As for the HW device, it can be observed that device performance was significantly reduced in proximity to the side walls of the chamber. However, both the extent of performance reduction and the width of the 'edge effect' were lower compared to the HW device.

We observed that addition of transversal bars to the metal frame, apart from stabilising the glass reflector, also resulted in a more homogeneous distribution of the force field across the fluid layer width. This was generally achieved at the expenses of the field strength in the central region of the channel, which however proved to be high enough to manipulate bacteria towards the glass reflector. The effect of transversal bars on the uniformity of the acoustic field in layered resonators is currently under investigation in our laboratories (both experimentally and computationally), and it will represent the subject of a separate manuscript. Fluid flow rate and US were re-activated in between individual *z*-scans, to ensure that each acquisition was performed under identical conditions.

The *z*-scan is able to resolve both the nodal position and distribution of bacteria in the fluid volume. The distribution of bacteria will reflect the averaged strength of the acoustic field over the path that bacteria have travelled to reach the measurement point, and is thus a useful tool for ensuring that this averaged force is relatively uniform across the device width; *e.g.* for the TR device, regions with a stronger acoustic field will create a distribution of bacteria that are closer to the reflector surface. A tight distribution also indicates that acoustic streaming is not causing significant disruption to the intended acoustic manipulation.

5. Conclusion

The importance of rapid and frequent water quality measurements is widely recognised.[8]

Acoustic manipulation of microorganisms is non-trivial, mainly due to the small bacterial size (~1 μm) and the associated reduction of acoustic radiation forces. At this dimensional scale, the drag forces associated with acoustic streaming or thermal convection may overcome the acoustic radiation forces.[77] Only few studies have previously reported on continuous-flow concentration of 1 μm diameter beads[49] or microorganisms[43] using HW resonators. In the latter case,

larger seed particles were used to increase the trapping efficiency by exploiting secondary acoustic radiation forces.

In this study we have investigated the thin reflector acoustic mode[31] and it has demonstrated a range of advantages compared to half-wavelength or quarter-wavelength resonators, including reduced sensitivity of the acoustic performance to variations in the reflector and fluid layers thickness,[31] and presence of positive forces directed towards the reflector surface from every location within the fluid layer.[65]

To achieve the desired performance, we adopted two key strategies: mechanically stabilising the glass thin reflector layer; and preventing bacterial adhesion to the reflector surface by modifying it with covalently attached coatings.

The optimised thin-reflector device allowed for significant increase in bacterial concentration to be achieved, at flow rates that are practical for the sample volumes found in online water quality analysis systems.

On the other hand, the performance of half-wavelength resonators was inferior, particularly at higher flow rate ratios. This was likely due to geometrical distortions of the nodal plane, and the presence of a strong lateral variation of the acoustic strength (*i.e.*, 'edge effect'). The latter was present also in thin-reflector resonators; however, it affected the acoustic levitation performance to a less extent. On-going work is focusing on the development of engineering solutions to minimise the impact of 'edge effect' on the concentration performance of thin-reflector resonators, and achieve a uniform strength of the acoustic field throughout the fluidic chamber.

It is worth mentioning that besides the analysis of water quality, the developed device could find a range of other applications in the field of pathogens detection, in either clinical or environmental assays, paving the way for the use of acoustofluidic technology in routine microbial detection. In order to facilitate the translation of the TR device into real-life applications, further developments to the system architecture could be implemented including (i) addition of flow control valves on the outlet lines to achieve passive flow regulation without the need for numerous pumps, and (ii) implementation of temperature regulation[78] or resonance frequency tracking[79] systems for stable operation of the device at higher acoustic powers. These could potentially result in a further increase of bacterial concentration performance.

Acknowledgements

The authors gratefully acknowledge Dr Maria Salta and Dr Natalya Doroshenko from the national Centre for Advanced Tribology at Southampton (nCATS; University of Southampton) for the support on bacterial culturing and sampling. This work was supported by funding from the European Research Council under the FP7 Program for the project AQUALITY (286601).

References

1 S. Gundry, R. Conroy and J. Wright, *J. Water Health*, 2003, **2**, 1–13.
2 J. Zhang, *J. Health Econ.*, 2012, **31**, 122–134.
3 T. Mattila-Sandholm and G. Wirtanen, *Food Rev. Int.*, 1992, **8**, 573–603.
4 R. Chmielewski and J. Frank, *Compr. Rev. Food Sci. Food Saf.*, 2003, **2**, 22–32.
5 W.H.O., *Burden of disease and cost-effectiveness estimates*, http://www.who.int/water_sanitation_health/diseases/burden/en/.
6 T. Clasen, W.-P. Schmidt, T. Rabie, I. Roberts and S. Cairncross, *BMJ*, 2007, **334**, 782.
7 A. V. Kneese and B. T. Bower, *Managing water quality: economics, technology, institutions*, Rff Press, 1984.
8 G. Kallis and D. Butler, *Water Policy*, 2001, **3**, 125–142.
9 K. A. Stevens and L.-A. Jaykus, *Crit. Rev. Microbiol.*, 2004, **30**, 7–24.
10 A. Aisopou, I. Stoianov and N. J. Graham, *Water Res.*, 2012, **46**, 235–246.
11 J. Vreeburg, P. Schaap and J. van Dijk, *Water Sci. Technol.: Water Supply*, 2004, **4**, 431–438.
12 S. Panguluri, G. Meiners, J. Hall and J. Szabo, *Distribution system water quality monitoring: Sensor Technology Evaluation - Methodology and Results*, US Environmental Protection Agency, Washington, DC, EPA/600/R-09/076, 2009.
13 J. Warrick, B. Casavant, M. Frisk and D. Beebe, *Anal. Chem.*, 2010, **82**, 8320–8326.
14 G. M. Whitesides, *Nature*, 2006, **442**, 368–373.
15 M. Nordin and T. Laurell, *Lab Chip*, 2012, **12**, 4610–4616.
16 B. H. Lapizco-Encinas, B. A. Simmons, E. B. Cummings and Y. Fintschenko, *Electrophoresis*, 2004, **25**, 1695–1704.
17 B. H. Lapizco-Encinas, R. V. Davalos, B. A. Simmons, E. B. Cummings and Y. Fintschenko, *J. Microbiol. Methods*, 2005, **62**, 317–326.
18 D. Puchberger-Enengl, S. Podszun, H. Heinz, C. Hermann, P. Vulto and G. A. Urban, *Biomicrofluidics*, 2011, **5**, 044111.
19 A. K. Balasubramanian, K. A. Soni, A. Beskok and S. D. Pillai, *Lab Chip*, 2007, **7**, 1315–1321.
20 S. Y. Kim, E. S. Lee, H. J. Lee, S. Y. Lee, S. K. Lee and T. Kim, *J. Micromech. Microeng.*, 2010, **20**, 095006.
21 N. R. Sharma, A. Lukyanov, R. L. Bardell, L. Seifried and M. Shen, Development of an evaporation-based microfluidic sample concentrator, in *Proc. SPIE 6886, Microfluidics, BioMEMS, and Medical Microsystems VI*, 2008.
22 J. Y. Zhang, J. Do, W. R. Premasiri, L. D. Ziegler and C. M. Klapperich, *Lab Chip*, 2010, **10**, 3265–3270.
23 J. Hawkes, M. Limaye and W. Coakley, *J. Appl. Microbiol.*, 1997, **82**, 39–47.
24 H. Bruus, *Lab Chip*, 2011, **11**, 3742–3751.
25 H. Mulvana, S. Cochran and M. Hill, *Adv. Drug Delivery Rev.*, 2013, **65**, 1600–1610.
26 P. Augustsson, C. Magnusson, M. Nordin, H. Lilja and T. Laurell, *Anal. Chem.*, 2012, **84**, 7954–7962.
27 D. Carugo, D. N. Ankrett, P. Glynne-Jones, L. Capretto, R. J. Boltryk, X. Zhang, P. A. Townsend and M. Hill, *Biomicrofluidics*, 2011, **5**, 044108.
28 W. Longsine-Parker, H. Wang, C. Koo, J. Kim, B. Kim, A. Jayaraman and A. Han, *Lab Chip*, 2013, **13**, 2144–2152.
29 S. Rodamporn, N. Harris, S. P. Beeby, R. J. Boltryk and T. Sanchez-Eisner, *IEEE Trans. Biomed. Eng.*, 2011, **58**, 927–934.

30 D. N. Ankrett, D. Carugo, J. Lei, P. Glynne-Jones, P. A. Townsend, X. Zhang and M. Hill, *J. Nanobiotechnol.*, 2013, **11**, 20.
31 P. Glynne-Jones, R. J. Boltryk, M. Hill, N. R. Harris and P. Baclet, *J. Acoust. Soc. Am.*, 2009, **126**, EL75–EL79.
32 M. Wiklund and H. M. Hertz, *Lab Chip*, 2006, **6**, 1279–1292.
33 J. J. Hawkes, M. J. Long, W. T. Coakley and M. B. McDonnell, *Biosens. Bioelectron.*, 2004, **19**, 1021–1028.
34 J. J. Hawkes and W. T. Coakley, *Enzyme Microb. Technol.*, 1996, **19**, 57–62.
35 J. J. Hawkes and W. T. Coakley, *Sens. Actuators, B*, 2001, **75**, 213–222.
36 J. J. Hawkes, R. W. Barber, D. R. Emerson and W. T. Coakley, *Lab Chip*, 2004, **4**, 446–452.
37 A. H. Yang and H. T. Soh, *Anal. Chem.*, 2012, **84**, 10756–10762.
38 A. Nilsson, F. Petersson, H. Jönsson and T. Laurell, *Lab Chip*, 2004, **4**, 131–135.
39 F. Petersson, L. Åberg, A.-M. Swärd-Nilsson and T. Laurell, *Anal. Chem.*, 2007, **79**, 5117–5123.
40 J. D. Adams, C. L. Ebbesen, R. Barnkob, A. H. Yang, H. T. Soh and H. Bruus, *J. Micromech. Microeng.*, 2012, **22**, 075017.
41 Y. Ai, C. K. Sanders and B. L. Marrone, *Anal. Chem.*, 2013, **85**, 9126–9134.
42 B. Hammarström, H. Yan, J. Nilsson and S. Ekström, *Biomicrofluidics*, 2013, **7**, 024107.
43 B. Hammarstrom, T. Laurell and J. Nilsson, *Lab Chip*, 2012, **12**, 4296–4304.
44 A. Lenshof, C. Magnusson and T. Laurell, *Lab Chip*, 2012, **12**, 1210–1223.
45 R. Townsend, M. Hill, N. Harris and N. White, *Ultrasonics*, 2004, **42**, 319–324.
46 K. Yasuda, S.-I. Umemura and K. Takeda, *Jpn. J. Appl. Phys.*, 1995, **34**, 2715–2720.
47 G. Goddard and G. Kaduchak, *J. Acoust. Soc. Am.*, 2005, **117**, 3440.
48 M. Hill, R. J. Townsend and N. R. Harris, *Ultrasonics*, 2008, **48**, 521–528.
49 N. Harris, M. Hill, R. Townsend, N. White and S. Beeby, *Sens. Actuators, B*, 2005, **111**, 481–486.
50 M. Evander, A. Lenshof, T. Laurell and J. Nilsson, *Anal. Chem.*, 2008, **80**, 5178–5185.
51 M. Wiklund, J. Toivonen, M. Tirri, P. Hanninen and H. M. Hertz, *J. Appl. Phys.*, 2004, **96**, 1242–1248.
52 L. A. Kuznetsova and W. T. Coakley, *J. Acoust. Soc. Am.*, 2004, **116**, 1956.
53 S. M. Hagsäter, T. G. Jensen, H. Bruus and J. P. Kutter, *Lab Chip*, 2007, **7**, 1336–1344.
54 R. Barnkob, P. Augustsson, T. Laurell and H. Bruus, An automated full-chip micro-PIV setup for measuring microchannel acoustophoresis: Simultaneous determination of forces from acoustic radiation and acoustic streaming, in *Proc. 14th International Conference on Miniaturized Systems for Chemistry and Life Sciences*, 2010.
55 R. Townsend, M. Hill, N. Harris and M. McDonnell, *Ultrasonics*, 2008, **48**, 515–520.
56 M. Antfolk, P. B. Muller, P. Augustsson, H. Bruus and T. Laurell, *Lab Chip*, 2014, **14**, 2791–2799.
57 L. Gorkov, *Dokl. Akad. Nauk SSSR*, 1961, **140**, 88–92.
58 A. Lenshof, M. Evander, T. Laurell and J. Nilsson, *Lab Chip*, 2012, **12**, 684–695.
59 P. Glynne-Jones, C. E. Demore, C. Ye, Y. Qiu, S. Cochran and M. Hill, *IEEE Trans. Sonics Ultrason.*, 2012, **59**, 1258–1266.
60 C. Woldringh, J. Binnerts and A. Mans, *J. Bacteriol.*, 1981, **148**, 58–63.
61 W. H. Grover, A. K. Bryan, M. Diez-Silva, S. Suresh, J. M. Higgins and S. R. Manalis, *Proc. Natl. Acad. Sci. U. S. A.*, 2011, **108**, 10992–10996.
62 A. Zipursky, E. Bow, R. S. Seshadri and E. J. Brown, *Blood*, 1976, **48**, 361–371.
63 S. J. Lighthill, *J. Sound Vib.*, 1978, **61**, 391–418.
64 J. Lei, P. Glynne-Jones and M. Hill, *Lab Chip*, 2013, **13**, 2133–2143.
65 P. Glynne-Jones, R. J. Boltryk and M. Hill, *Lab Chip*, 2012, **12**, 1417–1426.
66 P. Glynne-Jones, R. J. Boltryk and M. Hill, *Lab Chip*, 2012, **12**, 1417–1426.
67 M. Hill and R. J. Wood, *Ultrasonics*, 2000, **38**, 662–665.
68 M. Hill, Y. Shen and J. J. Hawkes, *Ultrasonics*, 2002, **40**, 385–392.
69 N. Stuurman, N. Amdodaj and R. Vale, *Microsc. Today*, 2007, **15**, 42–43.
70 C. A. Schneider, W. S. Rasband and K. W. Eliceiri, *Nat. Methods*, 2012, **9**, 671–675.
71 M. A.-S. Vigeant, R. M. Ford, M. Wagner and L. K. Tamm, *Appl. Environ. Microbiol.*, 2002, **68**, 2794–2801.
72 N. Mitik-Dineva, J. Wang, V. K. Truong, P. Stoddart, F. Malherbe, R. J. Crawford and E. P. Ivanova, *Curr. Microbiol.*, 2009, **58**, 268–273.
73 J. Palmer, S. Flint and J. Brooks, *J. Ind. Microbiol. Biotechnol.*, 2007, **34**, 577–588.
74 M. Salta, L. Capretto, D. Carugo, J. A. Wharton and K. R. Stokes, *Biomicrofluidics*, 2013, **7**, 064118.
75 O. Manneberg, B. Vanherberghen, B. Önfelt and M. Wiklund, *Lab Chip*, 2009, **9**, 833–837.
76 P. Glynne-Jones, R. J. Boltryk, N. R. Harris, A. W. Cranny and M. Hill, *Ultrasonics*, 2010, **50**, 68–75.
77 L. A. Kuznetsova and W. T. Coakley, *J. Acoust. Soc. Am.*, 2004, **116**, 1956–1966.
78 J. Svennebring, O. Manneberg and M. Wiklund, *J. Micromech. Microeng.*, 2007, **17**, 2469.
79 B. Hammarström, M. Evander, J. Wahlström and J. Nilsson, *Lab Chip*, 2014, **14**, 1005–1013.

